Precipitation of Calcium Carbonate Mineral Induced by Viral Lysis of Cyanobacteria: Evidence from Laboratory Experiments

Hengchao Xu[1, 2], Xiaotong Peng[2*], Shijie Bai[2, 3], Kaiwen Ta[2], Shouye Yang[1], Shuangquan Liu[2], Ho Bin Jang[3], Zixiao Guo[2]

[1]School of Ocean and Earth Science, Tongji University, Shanghai, China
[2]Deep-sea Science division, Institute of Deep-sea Science and Engineering, Chinese Academy of Science, Sanya, Hainan, China
[3]Department of Microbiology, The Ohio State University, Columbus, OH, USA

Correspondence to: X. Peng (xtpeng@idsse.ac.cn)

Abstract. Viruses have been acknowledged to be important components of the marine system for the past two decades, but their role in the functioning of the geochemical cycle has not been thoroughly elucidated to date. Virus induced rupturing of cyanobacteria is theoretically capable of releasing intracellular bicarbonate and inducing the homogeneous nucleation of calcium carbonate; however, experiment-based support for virus induced calcification is lacking. In this laboratory study, both water carbonate chemistry and precipitates were monitored during the viral infection and lysis of host cells. Our results show that viral lysis of cyanobacteria can influence the carbonate equilibrium system remarkably and promotes the formation and precipitation of carbonate minerals. Amorphous calcium carbonate (ACC) and aragonite were evident in the lysate, compared to the brucite precipitate in noninfected cultures, implying that a different precipitation process had occurred. Based on the carbonate chemistry change and microstructure of the precipitation, we propose that viral lysis of cyanobacteria can construct a calcification environment where carbonate is the dominant inorganic carbon species. Numerous virus particles available in lysate may coprecipitate with the calcium carbonate. The experimental results presented in this study, first demonstrate the pathway and result regarding how viruses influence the mineralization of carbonate minerals. It is suggested that virus calcification has open new perspectives on mechanisms of $CaCO_3$ biomineralization and may play a crucial role within the earth system.

1 Introduction

Cyanobacteria, which are ubiquitously abundant organisms and play important roles in most aquatic environments, are usually known to influence $CaCO_3$ precipitation by taking up inorganic carbon via photosynthesis (Obst et al., 2009b; Planavsky et al., 2009; Yang et al., 2016; Kamennaya et al., 2012; Kranz et al., 2010; Semesi et al., 2009; Riding, 2011; 2012; Merz-Preiß, 2000). Although there is great importance in calcium carbonate formation mediated by cyanobacteria in sedimentary deposits, the mechanisms involved are still controversial. In many cases, the precipitation of $CaCO_3$ by cyanobacteria has been invariably considered a noncontrolled process, promoted either by photosynthetic uptake of inorganic

carbon, raising the pH adjacent to cyanobacterial cells (Riding, 2006) or induced by cell-surface properties for the nucleation of $CaCO_3$ minerals (Obst et al., 2009b). In contrast, diverse cyanobacterial taxa have been shown recently to form amorphous calcium carbonate minerals intracellularly, with a diameter of several hundreds of nanometers (Couradeau et al., 2012; Benzerara et al., 2014). The intracellular carbonate makes the mechanisms involved in calcification more confusing (Cam et al., 2015; 2016; 2018; Li et al., 2016). Thus, new pathways, in which some biological processes alter the carbonate system, are important to evaluate.

Viruses, which are vital parasites of unicellular cyanobacteria, can modulate microbial production and, in some cases, can terminate plankton blooms (McDaniel et al., 2002; Bratbak et al., 1993; Bratbak et al., 1996; Suttle, 2005; 2007). It has been established that 3-31% of free-living bacteria are infected by viruses, which can occur in excess of 10^5 infectious units ml^{-1} (Suttle and Chan, 1994). Hence, viral lysis of microbes is certainly thought to have direct effects on both ecosystem function involving the release of nutrients back into the environment and the host-involved geochemical reaction (Brussaard et al., 2008; Rohwer and Thurber, 2009; Weitz and Wilhelm, 2012; Jover et al., 2014).

The thermodynamic calculation proposed by Lisle and Robbins (2016) infers that virus induced cyanobacteria lysate theoretically can elevate the saturation index of carbonate minerals at the cellular level, by releasing cytoplasmic-associated bicarbonate. This thermodynamic calculation also highlights that the released cytoplasm-associated bicarbonate can be as much as ~23-fold greater than in the surrounding seawater, which can shift the carbonate chemistry toward the homogenous nucleation of calcium carbonate (such as vaterite). However, theoretical calculations do not take into account the condition that magnesium may influence the properties and behaviors of carbonate in seawater (Morse et al., 2007). Displacements of acid-base carbonic equilibrium in seawater can not only form calcium carbonate minerals, but also can lead to the precipitation of $Mg(OH)_2$ (brucite) (Möller, 2007). It has been proposed that the dissolution of brucite in seawater is favourable for $CaCO_3$ precipitation (Nguyen Dang et al., 2017).

Furthermore, viral particles could act as nucleation sites for precipitation of different minerals. In the past few years, researchers have investigated the theory that the capsid of viruses can interact directly with elements in solution, and thus, potentially mediate the formation and precipitation of different minerals (Daughney et al., 2004; Kyle et al., 2008; Peng et al., 2013; Pacton et al., 2014; De Wit et al., 2015; Laidler and Stedman, 2010; Orange et al., 2010). Virus-related carbonate minerals are also reported in recent studies of biofilms from hypersaline lakes, where hypersaline carbonate minerals can precipitate at the surface of viral particles (Pacton et al., 2014; Lisle and Robbins, 2016; Perri et al., 2017). However, the pathway of precipitation of calcium carbonate onto the surface of virus remains poorly understood. When combined with the release of cytoplasm-associated bicarbonate, which results in the formation of carbonate mineral energetically favored, and available viral capsids for surface-induced precipitation, the comprehension of viral influence on the precipitation of carbonate is extremely limited.

Laboratory studies of viral calcification were adopted here by culturing viruses and their host *Synechococcus* spp. PCC 7177. Such modeling experiments do not intend to mimic the processes occurring within the cells, which remain unknown, and generally do not provide an ultimate and direct answer as to which geobiological processes are involved in

biomineralization. However, these experiments constrain, to some extent, the chemical conditions necessary to predict the geochemical processes similar to those in the aquatic environment. Carbonate parameters and cultural status were monitored to calculate the carbonate equilibrium system and saturation index. Precipitates of the culture were also characterized, to identify the microstructure of the minerals. Our results provide large-scale support of the importance of carbonate formation and precipitation during virus induced cyanobacteria mortality. The extension of the viral role in mediating carbonate systems will also provide an important mechanisms of $CaCO_3$ biomineralization in the earth system

2 Methods and Materials

2.1 Cyanobacteria and Viruses

Cyanobacteria, which have a long evolution history and are widespread in the marine environment, are key primary producers in the surface of the world ocean system. *Synechococcus* sp. PCC 7177 and the viruses that infected it were isolated from surface seawater from Sanya Bay (Supplement material). *Synechococcus* is a unicellular cyanobacterium that is very widespread in the marine environment and thus, is well-adapted for the present experiment (Fig. S1). Isolated virus particles, which are ~53 nm in diameter (Fig. S2), are classified as podovirus, based on morphology and metagenomic analysis (Fig. S3).

2.2 Culture conditions and calcification experiments

Cyanobacteria and viruses were grown at 25°C, under a photon irradiance of 6000 lux, with a 12 h light/dark cycle (Yang et al., 2016). Before the precipitation experiments, cyanobacteria were cultivated to harvest fresh cells for calcification experiments. Precipitation experiments were performed in sterile 4-L borosilicate bottles, in 0.2-μm-filtered artificial medium (based on F/2 media, Table 1). To minimise gas exchange with air, filtration was performed by means of a peristaltic pump. To avoid artifacts caused by residues from previous precipitation experiments, the bottles were treated overnight in 0.1 M hydrochloric acid, rinsed with water several times and finally, stored overnight filled with water. 2000 ml of medium was added into each bottle. The headspaces of the bottle were continuously exchanged with ambient air via a plastic membrane. The inoculation and subsampling of each experiment was performed aseptically.

Two milliliters of fresh cells from the precultures was inoculated into each of 2 L of culture media. After the lag phase (day 5), 5 ml of viral stock (~10^9 virus particles per milliliter) was inoculated in one treatment (Group A) to detect the potential viral influence on carbonate chemistry. The other treatment without inoculation of viruses was left as a control (Group B). Both treatments were run in duplicate, and subsamples from these incubations were taken simultaneously over the course of the incubations.

During the course, subsamples were taken from both treatments for analysis of the cell and virus concentration, total alkalinity (TA), dissolved inorganic carbon (DIC), calcium and magnesium concentration, and morphology of minerals. First, salinity was determined by measuring the apparent electrical conductivity. Cells and viruses were enumerated with a

1.5 ml solution. Filtrates (through 0.22 μm filters) were collected for TA, DIC, calcium and magnesium analysis. TA samples (30 ml) were stored in borosilicate bottles at room temperature. DIC samples (5 ml) were stored in borosilicate flasks without headspace at 4 °C. Subsamples for DIC and TA were poisoned with $HgCl_2$ solution to inhibit growth (Cao and Dai, 2011). At the end of the stationary phase (day 16), the particulate fraction of the medium (~1 L) was harvested via centrifugation (13000 g, 5 min) for electronic microscopy and X-ray diffraction study, using the methods adopted from Peng et al. (2013).

2.3 Measuring methods

2.3.1 Total alkalinity and dissolved inorganic carbon

Total alkalinity (TA) was determined by titration of 25.00 ml of medium samples with HCl solution from the volume of HCl required. The instrument and program ran automatically by *Metrohm* 916 Ti-Touch. The approximately 0.1 N HCl solution was ascertained by titration of solutions made from dried high-purity sodium carbonate and borax. The fluctuations of our total alkalinity determinations were approximately limited to 10 μM/kg.

DIC was measured by acidification of 0.5-1.0 ml of water samples at the Stable Isotope Laboratory, Third Institute of Oceanography, State Oceanic Administration, China. Measurements were performed with continuous flow isotope ratio mass spectrometry (Delta V Advantage, Thermo-Fisher Scientific Inc., USA), coupled with a GasBench II device.

2.3.2 Calcium and magnesium cations

Concentration of magnesium and calcium cations were determined by ion chromatography (*Dionex* ICS-900), after acidification by 1 N HCl. The precision of the IC method used was 2 ppm for Ca^{2+} and 5 ppm for Mg^{2+}.

2.3.3 Enumeration of cells and viruses

For determination of cell numbers, samples of 0.5ml were filtered on black nuclepore filters (25 mm, 0.2μm pore size, Whatman) under low vacuum (200 mbar). Cyanobacteria were counted within 72h under a *Leica* fluorescence microscope (Leica DM6B) with autofluorescence. The growth curves of the cultures were drawn through constant survival cell counts.

Enumeration of viruses from the culture was following Patel et al., (2007). Subsamples were first filtered (25 mm, 0.2μm pore size, Whatman, Inc.) to remove bacteria and large mineral particles. Aliquots of filtered supernatant were filtered through 0.02μm- poresize Anodisc 25 membrane filter (Whatman, Inc.). The Anodisc filters were then stained with a final concentration of 25X SYBR Green for 15 min, mounted on glass microscope slides, and treated with an antifade solution. The slides were examined using an epifluorescence microscope (Leica DM6B) within 72 h. A minimum of 10 fields of view was examined per slide.

2.3.4 Electron microscopy

Subsamples for the TEM study were fixed by the addition of glutaraldehyde (to 4% final concentration); they were then rinsed in distilled water to remove salts, mounted on copper grids and air-dried. The TEM analysis was conducted on a JEM-2100F field emission electron microscope operated at an accelerating voltage of 200 kV. Elemental analysis was conducted at 200 kV using an Oxford INCA Energy TEM X-ray energy dispersive spectrometer. Elemental maps were acquired in a

STEM DF mode operating at 200 kV, with a focused electron beam (1 nm). The mineralogy of the structures in the areas of interest were determined using selected-area electron diffraction (SAED).

For SEM analysis, dried precipitates were fixed onto aluminum stubs with two-way adherent abs and allowed to dry overnight. The samples were carbon-coated and examined with an Apreo scanning electron microscope (Thermofisher Scientific).

2.3.5 X-ray Diffraction

XRD was employed to characterize the bulk mineralogy of the precipitates. The subsamples were thoroughly ground, followed by analyses using a LabX XRD-6100 X-ray Diffractometer with Cu Kα radiation (λ = 1.54056 nm) and a 2θ angle in the range of 10° to 80° at a speed of 1° min^{-1}.

2.4 Saturation indices calculation

To determine the activity of the carbonate species and the degree of saturation in the solutions sampled, the geochemical computer program PHREEQC Interactive [version 3.3; Wateq4f database; United States Geological Survey (USGS), Reston, VA, USA] was used (Obst et al., 2009b). Speciation of the carbonate system and saturation state of medium relative to a set of minerals were modelled for each of the subsample solution. The saturation index (SI) is defined as SI = log[IAP/K_{sp} Mineral], where IAP is the ion activity product (For $CaCO_3$, IAP= [Ca^{2+}][CO_3^{2-}]) and K_{sp} represents the solubility product for a given temperature. The pH values of subsamples were calculated by desired total alkalinity, which were measured in 2.3.1.

3 Results

3.1 Growth of cyanobacteria culture

The color of the culture medium varied daily between the two treatments after virus induced lysis. The supernatant of Group A, which was inoculated to allow the adsorption and infection of cyanobacteria, became clarified on the 14th day and seemed completely clear on the 17th day (Fig. 1b, d). Group B, in contrast, had some turbidity and higher cell density at the corresponding times (Fig. 1a, c). By the time cells were lysed, the white precipitation phase emerged in Group A (Fig. 1b, d). Cell growth was monitored over the course of 20 days by counting the autofluorescence of cyanobacteria. After the inoculation, cells exhibited a lag phase and started to grow exponentially for 9 to 13 day before reaching maximum cell numbers (Fig. 2a). The cell abundance of Group A was slightly lower than Group B on the fifth day to eighth day (Fig. 2a). Although the cell abundance increased at the first few days, the growth rates of Group A were slightly lower and the cell number was reduced to 1.7×10^7 cell/ml, compared to the 1.3×10^8 cell/ml of Group B (days 19, Fig. 2a). The maximum number of virus particles occurred on the 9th day (Fig. 2a). Unlike the traditional viral one-step growth curve, virus particle in the present calcification experiment decreased with the ongoing process of calcification. The burst size of virus can be estimated by calculating the ratio of viral particles to the number of killed host cells over the short-time intervals. The lysed cells were estimated either by

decrease of bacteria number in Group A or increase of bacteria number in Group B (Days 8-9). Two estimations came up with similar results that the burst size is 3.01-3.29.

3.2 Change of carbonate parameters

The carbonate chemistry of the two treatments showed similar patterns during the first 10 days, but started to deviate strongly in terms of the total alkalinity (TA) and dissolved inorganic carbon (DIC) afterwards, when the cell lysis rates were greater than cell replication rates in Group A (Fig. 2b, c). In Group B, there was a negative correlation between DIC and cell growth which was a reflection of photosynthetic carbon uptake (Fig. 2a, c). When cultures were at the end of the exponential phase (Group B, days 14), the DIC declined to the lowest values. In group A, by contrast, the lowest DIC values was found on the 12th day, when the lytic rate began to dominate cell replication. DIC then rose to the initial level, because of re-equilibration with the atmosphere in the present open system. The TA of the two treatments also dropped during the exponential phase, reflecting a removal of cations from the solution (Fig. 2b). Compared to Group A, TA in Group B dropped to the lower level. During the lytic phase in Group A, TA increased again to values of 2936 μmol/kg in three days and maintained balance during the lytic cycle. Both calcium and magnesium cations were removed from the solution at the early-exponential growth phases (Fig. 3). It is interesting to find that precipitated calcium redissolved into the solution in Group B. In striking contrast, there was a persistent calcium removal within the viral lysate, indicating that robust virus-induced calcification had occurred (Fig. 3 a, b).

3.3 Microstructure of virus-induced carbonate precipitation

SEM and TEM images of the white precipitates from the viral lysate showed numerous calcium nanoparticles scattered or aggregated. These particles were in a spherical morphology, having diameters ranging from dozens of nanometers to hundreds of nanometers (Fig. 4, 5). STEM mappings and XEDS analysis showed evidence of calcium accumulation all around the particle surface (Fig. 5), as well as selected-area electron diffraction (SAED) patterns with diffuse halos (Fig. 5b), confirming that they were amorphous calcium carbonate (ACC) (Rodriguez-Blanco et al., 2008). Although Mg was not dominant in the particles, there were signs of enrichment of Mg around the particles (Fig. 5c). SEM images of the nanoparticle are attached to the surface of the infected cells and usually have an encrusted structure (Fig. 4d). The bulk mineralogy of the cultural deposits, based on XRD analyses, were dominated by brucite in the noninfection treatment, compared to aragonite in the lysate (Fig. 6).

4 Discussion

4.1 Carbonate chemistry influenced by the growth of cyanobacteria

Various studies in recent years have demonstrated the direct effects of carbonate chemistry shifts over the course of cyanobacteria growth (Dittrich et al., 2003; Kranz et al., 2010; Millo et al., 2012; Obst et al., 2009b; Yang et al., 2016). In

cases where photosynthesis occurred, this results in the stimulation of cell division and DIC uptake, but no total alkalinity changes because no other sources of base are added during photosynthetic carbon uptake:

$$HCO_3^- + H_2O \rightarrow CH_2O + OH^- + O_2 \quad (1)$$

Studies of cyanobacteria calcification always attribute the increase of pH to the growth of cyanobacteria which construct a favorable calcification environment where carbonate is the dominant inorganic carbon species and induces calcification by the incorporation of carbonate ions into a growing $CaCO_3$ crystal (Lee et al., 2004; Obst et al., 2009a; Kranz et al., 2010). It has been interpreted by the majority of studies that cyanobacteria calcification is restricted to certain species (Merz-Preiß, 2000; Lee et al., 2004). The calcification induced by photosynthetic acid-base equilibrium by *Synechococcus* sp. PCC 7177 in the present study seems to be transitional and unable to calcify to the extent that stable $CaCO_3$ precipitates are formed. This is inferred based on the observation that cations are released again into the solution in Group B. Fixed Ca^{2+} redissolves to the concentration equivalent to the former concentration (Fig. 3a). On the 8th day, however, there was an evident decrease in calcium concentration, accompanied by a decrease of TA, which implies that calcium carbonate was formed and separated from the filtrate (Fig. 3a). Photosynthetic carbon uptake (Equation 1) raised the pH values of the medium, leading to the formation of $CaCO_3$. This $CaCO_3$ phase can be recognized as amorphous calcium carbonate, based on electron microscope images (Fig. 4, 5) and the fact that it is unstable. ACC, which received relatively little attention as one of metastable $CaCO_3$ phases, has been increasingly recognized as a precursor for the formation of crystalline calcium carbonate (Cartwright et al., 2012; Weiner and Addadi, 2011). ACC may precipitate virtually instantaneously, when conditions promote high local supersaturation for short periods of time (Blue et al., 2017; Cartwright et al., 2012). Although the saturation index (SI) of the ACC <0 (Table 2), implying nonspontaneous ACC formation within the solution, the growth of cyanobacteria in the present experiment created an ACC favorable microenvironment on days 8-10, reflected by the removal of Ca^{2+}.

Magnesium, which is actually precipitated as brucite from the solution, is also responsible for removing TA from the cyanobacteria culture. It has been demonstrated that supersaturated $Mg(OH)_2$ can precipitate at local alkaline conditions with pH > 9.30 (Möller, 2007). Saturation indices (SI), which are determined using the software PHREEQC, yielded values > 0 for brucite ($Mg(OH)_2$) during the first 8 days (0.34 ~ 1.15) and values < 0 after the 10th day (-1.47 ~ -0.15) in Group B (Table 2). As DIC transportation by cyanobacteria proceeded, the pH of the growth medium increased (Table 2, S1), thus, leading to the formation of $Mg(OH)_2$ in the supersaturated state (Equation 1 and 2). The emergence of brucite crystal formation have also been reported in coral microbial biofilms (Nothdurft et al., 2005) and cultures of diatoms (Tesson et al., 2008), where high pH and low pCO_2 microenvironments are created by biological activities such as the cyanobacteria in the present study.

$$Mg^{2+} + 2OH^- \rightarrow Mg(OH)_2 \quad (2)$$

Upon the mass consumption of DIC by photosynthesis and fixation of calcium, cell growth seems to slow down (days 8-9, Fig. 2a). In the present open system, atmospheric CO_2 is dissolved in water and changes the acid-base balance of the system. Dissolved carbon is present in the form of bicarbonate at the present pH level:

$$2CO_2 + CO_3^{2-} + OH^- + H_2O \rightarrow 3HCO_3^- \quad (3)$$

The reaction represented by equation 3 in Group B, based on the continuous decrease of DIC (days 10-14). On days 9 ~10, there is an insufficient amount of carbon for photosynthetic carbon to be concentrated in the form of CO_2 or HCO_3^- (Miller et al., 1990). Nevertheless, cyanobacteria grew vigorously during days 10 -14 (Fig. 2a). The consumption of CO_3^{2-} and OH^- led the unstable minerals, such as ACC and brucite, to dissolve in the solution. Especially for the ACC, robust carbon concentration inhibits the transformation of ACC to a more stable carbonate phase such as aragonite. pH values calculated by PHREEQC after the 10th day were reduced to 8.66, at which $Mg(OH)_2$ formation cannot occur spontaneously. Consequently, with the growth of cyanobacteria, carbonate alkalinity limitation leads to the redissolution of calcium and magnesium minerals.

4.2 Carbonate chemistry influenced by viral lysis of cyanobacteria

It seems that the two treatments of the tested culture grew at similar rates and reached similar cell densities during the first 8 days, despite inoculation with the viruses (Fig. 2a). However, when lytic rates ran over the bacterial replication (day 8), Mg^{2+} began to recover to the initial level, but Ca^{2+} was further removed simultaneously presenting distinct variations between the two treatments.

In regard to magnesium, which is immobilized from the solution in the form of brucite, the resulting mineral grains are unstable. It has been suggested that brucite may not be preserved over longer time frames, possibly being dissolved in the undersaturated state (Nothdurft et al., 2005). There is a strong positive correlation between Mg^{2+} and DIC recovered after the 12th day in Group A, which is the time point when the lytic rate begins to dominate cell replication. In the present open system, atmospheric CO_2 is dissolved in water and changes the acid-base balance of the system. Hence, brucite can dissolve with acidification during the culture of cyanobacteria:

$$Mg(OH)_2 + CO_2 \rightarrow Mg^{2+} + HCO_3^- + H_2O \quad (4)$$

The release of extra bicarbonate releasing during the dissolution of brucite also contributes to the TA recovery after the 12th day.

On the other hand, it should be noted that, with the aid of the virus, photosynthetic uptake of inorganic carbon decreases. Calcium, which is in the form of ACC during the growth of cyanobacteria, is formed in a stable carbonate environment, where Equation 3 cannot take place (days 8-12). The atmospheric CO_2 exchange is neutralized by $Mg(OH)_2$, as discussed above (days 12-16). Brucite dissolution in seawater controls the pH and Mg/Ca ratios and is recognized as a key factor

inhibiting calcite and vaterite growth and precipitation (Nguyen Dang et al., 2017). Thus, a microenvironment favorable for calcification is available after the viral lysis of cyanobacteria and deposition of aragonite carbonate minerals.

4.3 Virus induced carbonate precipitation

The aggregates of aragonite in viral lysate were confirmed by the means of XRD (Fig. 6). It has been extensively investigated that various physicochemical factors control the formation of the $CaCO_3$ polymorph and aragonite tends to precipitate under a high molar ratio of Mg/Ca (Folk, 1974; Berner, 1975). Nevertheless, the microenvironment maintained by the growth of *Synechococcus* sp. PCC 7177 could not overcome the activation energy barriers for the formation of aragonite, according to the evidence presented by XRD and the carbonate chemistry changes in Group B. TEM images revealed no order in the majority of the detected particles (Fig. 4, 5), which was confirmed by the diffuse rings in the selected area electron diffraction patterns and the appearance of nanodomains within the ACC particles (Rodriguez-Blanco et al., 2008). Unlike Group B, with the aid of the viral cycle and the lysis of the host, the dissolution of carbonate seemed not to occur, and a more stable mineral formed in Group A.

Here, a possible model for calcium carbonate precipitation induced by viral lysis of cyanobacteria is proposed by regarding the carbonate chemical changes and microstructures (Fig. 7). As bicarbonate transport by cyanobacteria and intracellular conversion to CO_2 for photosynthesis proceeded, the pH of the ambient waters increased, leading to the formation of brucite and ACC. If no viruses were available, cell growth and replication would consume the bicarbonate. Atmospheric CO_2 dissolves in water but cannot do so in the form of CO_2 or HCO_3^- for photosynthesis, because of the high pH. Alternatively, dissolved CO_2 reacts with OH^- and $Mg(OH)_2$ resulting in dissolved carbon in the form of HCO_3^- for cyanobacteria. However, when cells are infected by viruses, there are a few percentages of uninfected cells that require bicarbonate. Only $Mg(OH)_2$ dissolved to neutralize the dissolution of CO_2 and precipitation of calcium carbonate will continue.

Preliminary investigations have also demonstrated that viruses from hypersaline lakes are incorporated in biogenic carbonate, suggesting that viruses may be mistaken for nanobacteria and may play a role in initiating calcification (De Wit et al., 2015; Pacton et al., 2014; Perri et al., 2017). The viral drive during the biogenic carbonate precipitation in hypersaline lakes is attributed to either an indirect route, involving silicified viruses as an intermediate phase during diagenesis (Pacton et al., 2014) or a direct incorporation of amino acids polymerized with viral proteins into growing high-Mg calcite crystals (De Wit et al., 2015). The encrusted structure indicated by SEM images may support the hypothesis of carbonate formation on and near the virus particles (Fig. 4d). Coprecipitation of viruses and calcium carbonate is also supported by the number of viruses floating in the solution. Subsamples for enumeration of virus particles were filtered to remove precipitated minerals. The yield of the filtrate may preclude viruses incorporated in minerals. This is a reasonable explanation as to why virus numbers did not increase exponentially, despite the bursting of host cells (Fig. 2a). Viral infection does not result in the immediate lysis of the host cell; dormancy occurs, while integrating their genome with host DNA and the replication along with it is relatively harmless. When the reproductive cycle initiates, the virus attacks and breaks down the cell wall peptidoglycan, which is an

essential structure that protects the cell protoplast from mechanical damage and from osmotic rupture (Middelboe and Jørgensen, 2006). Thus, we propose that Ca^{2+} has unfettered access to the intracellular space and reacts with cytoplasmic alkalinity (Fig. 7). When Ca^{2+} access to intracellular space, the existence of the capsid synthetized by viral DNA provides a surface for the initial calcification (Fig. 7). Calcification involves the addition of material to the preexisting viral surfaces, which may be similar to the mineralized virus in microbial mat from hot springs (Peng et al., 2013) or hypersaline lakes (Pacton et al., 2014; De Wit et al., 2015; Perri et al., 2017).

The pathway of virus-induced calcification during the lysis of the host cells was determined by experimental study and expands the mechanisms of $CaCO_3$ biomineralization. Perhaps, it is helpful to recognize the recent identification of accounted fractions of marine calcium carbonate particles in seawater (Heldal et al., 2012). Owing to the fact that biologically mediated $CaCO_3$ precipitation is one of the fundamental processes in the carbon cycle (Ridgwell and Zeebe, 2005; Planavsky et al., 2009; Riding, 2011; Kamennaya et al., 2012), the study of viral impact is important in an understanding of the carbon cycling on both the global and regional scales. For example, so-called “Whiting events”, which refers to events of high levels of suspended, fine-grained $CaCO_3$ precipitation, have long been spectacular and extensively investigated $CaCO_3$ precipitation events due to their controversial origin (Wright and Oren, 2005; Morse et al., 2003). Clear evidence of net carbonate precipitation from the waters culturing cyanobacteria and viruses suggest that release of the virus during plankton bloom may stimulate virus-induced $CaCO_3$ precipitation, representing one potential whiting mechanism for CO_2 sequestration. Furthermore, in view of the virus-induced carbonate deposition and the increased Mg/Ca ratio of the medium (Fig. 3c), the possibility that viral processes alter seawater Mg/Ca rations, which are an important proxy for reconstructing the paleoenvironment (Lear et al., 2000), is thus important to evaluate.

5 Conclusion

First, we provide a detailed view of changes in carbonate chemistry and mineral composition during viral infection and lysis of cyanobacteria. Amorphous calcium carbonate and aragonite were evident in the lysate, which differed substantially from the lack of calcification in the noninfected culture. We inferred that viral lysis of cyanobacteria can construct an environment of calcification, where carbonate is the dominant inorganic carbon species. Moreover, potential mechanisms involving viruses acting as nucleation sites are also discussed. Altogether, our results expand the role of viruses in mediating geochemical cycles and provide new perspectives on mechanisms of $CaCO_3$ biomineralization.

Data availability. Data used to generate Figs. 2, 3 are listed in the appendices. Genomic sequences are archived in an open-access database: https://submit.ncbi.nlm.nih.gov/subs/?search=SUB4436587

Author contributions: This work was designed by HX, XP and SY. Experimental work was performed by HX, SB, KT, SL and ZG. SB and HJ analysed genomic sequences. HX and SB led the writing of the papers and prepared the figures with contributions from all co-authors.

Competing interests. The authors declare that they have no conflict of interest.

Acknowledgments

Authors would like to acknowledge Dr. Dezhang Ren at Shanghai Jiaotong University for his help with the XRD analysis. The authors are also indebted to Ms Ling Li and Dr. Weijia Zhang at the Institute of Deep-sea Science and engineering for their assistance with cyanobacteria identification. Financial support for this research came from the "National Key R&D Program of China" (Grant NO. 2018YFC0309802), the "National Natural Science Foundation of China" (Grant NO. 41506139 and 41506097), "Strategic Priority Research Program" of the Chinese Academy of Science (Grant NO. XDB06020000), "National Key Basic Research Program of China" (Grant NO. 2015CB755905), and the "Natural Science Foundation of Hainan Province, China" (Grant NO. 20164175). We are greatly indebted to two anonymous journal reviewers and the journal associate editor, Lennart de Nooijer, for their critical comments on an earlier version of this manuscript.

References

Benzerara, K., Skouripanet, F., Li, J., Ferard, C., Gugger, M., Laurent, T., Couradeau, E., Ragon, M., Cosmidis, J., and Menguy, N.: Intracellular Ca-carbonate biomineralization is widespread in cyanobacteria, P. Natl. Acad. Sci. USA., 111, 10933-10938, https://doi.org/10.1073/pnas.1403510111, 2014.

Berner, R. A.: The role of magnesium in the crystal growth of calcite and aragonite from sea water, Geochim. Cosmochim. Acta., 39, 489-504, https://doi.org/10.1016/0016-7037(75)90102-7, 1975.

Blue, C. R., Giuffre, A., Mergelsberg, S., Han, N., De Yoreo, J. J., and Dove, P. M.: Chemical and physical controls on the transformation of amorphous calcium carbonate into crystalline $CaCO_3$ polymorphs, Geochim. Cosmochim. Acta., 196, 179-196, https://doi.org/10.1016/j.gca.2016.09.004, 2017.

Bratbak, G., Egge, J. K., and Heldal, M.: Viral mortality of the marine alga *Emiliania huxleyi* (Haptophyceae) and termination of algal blooms, Mar. Ecol. Prog. Ser., 93, 39-48, https://doi.org/10.3354/meps093039, 1993.

Bratbak, G., Wilson, W., and Heldal, M.: Viral control of *Emiliania huxleyi* blooms?, J. Marine. Syst., 9, 75-81, https://doi.org/10.1016/0924-7963(96)00018-8, 1996.

Brussaard, C. P., Wilhelm, S. W., Thingstad, F., Weinbauer, M. G., Bratbak, G., Heldal, M., Kimmance, S. A., Middelboe, M., Nagasaki, K., and Paul, J. H.: Global-scale processes with a nanoscale drive: the role of marine viruses, ISME J., 2, 575-578, https://doi.org/10.1038/ismej.2008.31;, 2008.

Cam, N., Georgelin, T., Jaber, M., Lambert, J. F., and Benzerara, K.: In vitro synthesis of amorphous Mg-, Ca-, Sr- and Ba-carbonates: What do we learn about intracellular calcification by cyanobacteria?, Geochim. Cosmochim. Acta., 161, 36-49, http://doi.org/10.1016/j.gca.2015.04.003, 2015.

Cam, N., Benzerara, K., Georgelin, T., Jaber, M., Lambert, J.-F., Poinsot, M., Skouri-Panet, F., and Cordier, L.: Selective uptake of alkaline earth metals by Cyanobacteria forming intracellular carbonates, Environ. Sci. Technol., 50, 11654-11662, https://doi.org/10.1021/acs.est.6b02872, 2016.

Cam, N., Benzerara, K., Georgelin, T., Jaber, M., Lambert, J. F., Poinsot, M., Skouri-Panet, F., Moreira, D., López-García, P., Raimbault, E., Cordier, L., and Jézéquel, D.: Cyanobacterial formation of intracellular Ca-carbonates in undersaturated solutions, Geobiology, 16, 49-61, https://doi.org/10.1111/gbi.12261, 2018.

Cao, Z., and Dai, M.: Shallow-depth $CaCO_3$ dissolution: Evidence from excess calcium in the South China Sea and its export to the Pacific Ocean, Global Biogeochem. Cy., 25, GB2019, https://doi.org/10.1029/2009GB003690, 2011.

Cartwright, J. H. E., Checa, A. G., Gale, J. D., Gebauer, D., and Sainz-Díaz, C. I.: Calcium carbonate polyamorphism and its role in biomineralization: How many amorphous calcium carbonates are there?, Angewandte Chemie., 51, 11960-11970, https://doi.org/10.1002/anie.201203125, 2012.

Couradeau, E., Benzerara, K., Gérard, E., Moreira, D., Bernard, S., Brown, G. E., and López-García, P.: An early-branching microbialite cyanobacterium forms intracellular carbonates, Science, 336, 459-462, https://doi.org/10.1126/science.1216171, 2012.

Daughney, C. J., Châtellier, X., Chan, A., Kenward, P., Fortin, D., Suttle, C. A., and Fowle, D. A.: Adsorption and precipitation of iron from seawater on a marine bacteriophage (PWH3A-P1), Mar. chem., 91, 101-115, https://doi.org/10.1016/j.marchem.2004.06.003, 2004.

De Wit, R., Gautret, P., Bettarel, Y., Roques, C., Marlière, C., Ramonda, M., Nguyen Thanh, T., Tran Quang, H., and Bouvier, T.: Viruses occur incorporated in biogenic high-Mg calcite from hypersaline microbial mats, PLoS ONE, 10, e0130552, https://doi.org/10.1371/journal.pone.0130552, 2015.

Dittrich, M., Müller, B., Mavrocordatos, D., and Wehrli, B.: Induced calcite precipitation by cyanobacterium *Synechococcus*, Acta hydrochimica et hydrobiologica, 31, 162-169, https://doi.org/10.1002/aheh.200300486, 2003.

Folk, R. L.: The natural history of crystalline calcium carbonate: effect of magnesium content and salinity, J. Sediment. Res., 44, 40-53, https://doi.org/10.1306/74d72973-2b21-11d7-8648000102c1865d, 1974.

Heldal, M., Norland, S., Erichsen, E. S., Thingstad, T. F., and Bratbak, G.: An unaccounted fraction of marine biogenic $CaCO_3$ particles, PLoS ONE, 7, 2012.

Jover, L. F., Effler, T. C., Buchan, A., Wilhelm, S. W., and Weitz, J. S.: The elemental composition of virus particles: implications for marine biogeochemical cycles, Nat. Rev. Micro., https://doi.org/12, 519-528, 10.1038/nrmicro3289, 2014.

Kamennaya, N., Ajo-Franklin, C., Northen, T., and Jansson, C.: Cyanobacteria as Biocatalysts for Carbonate Mineralization, Minerals, 2, 338, 2012.

Kranz, S. A., Gladrow, D. W., Nehrke, G., Langer, G., and Rosta, B.: Calcium carbonate precipitation induced by the growth of the marine cyanobacteria Trichodesmium, Limnol. Oceanogr., 55, 2563-2569, https://doi.org/10.4319/lo.2010.55.6.2563, 2010.

Kyle, J. E., Pedersen, K., and Ferris, F. G.: Virus mineralization at low pH in the Rio Tinto, Spain, Geomicrobiol. J., 25, 338-345, https://doi.org/10.1080/01490450802402703, 2008.

Laidler, J. R., and Stedman, K. M.: Virus silicification under simulated hot spring conditions, Astrobiology, 10, 569-576, https://doi.org/10.1089/ast.2010.0463, 2010.

Lear, C. H., Elderfield, H., and Wilson, P. A.: Cenozoic deep-sea temperatures and global ice volumes from Mg/Ca in benthic foraminiferal calcite, Science, 287, 269-272, https://doi.org/10.1126/science.287.5451.269, 2000.

Lee, B. D., Apel, W. A., and Walton, M. R.: Screening of cyanobacterial species for calcification, Biotechnol. Progr., 20, 1345-1351, https://doi.org/10.1021/bp0343561, 2004.

Li, J., Margaret Oliver, I., Cam, N., Boudier, T., Blondeau, M., Leroy, E., Cosmidis, J., Skouri-Panet, F., Guigner, J.-M., Férard, C., Poinsot, M., Moreira, D., Lopez-Garcia, P., Cassier-Chauvat, C., Chauvat, F., and Benzerara, K.: Biomineralization patterns of intracellular carbonatogenesis in Cyanobacteria: Molecular Hypotheses, Minerals, 6, 10, https://doi.org/10.3390/min6010010, 2016.

Lisle, J. T., and Robbins, L. L.: Viral lysis of photosynthesizing microbes as a mechanism for calcium carbonate nucleation in seawater, Front. Microbiol., 7, https://doi.org/10.3389/fmicb.2016.01958, 2016.

McDaniel, L., Houchin, L. A., Williamson, S. J., and Paul, J. H.: Plankton blooms: Lysogeny in marine *Synechococcus*, Nature, 415, 496-496, 2002.

Merz-Preiß, M.: Calcification in Cyanobacteria, in: Microbial Sediments, edited by: Riding, R. E., and Awramik, S. M., Springer Berlin Heidelberg, Berlin, Heidelberg, 50-56, 2000.

Middelboe, M., and Jørgensen, N.: Viral lysis of bacteria: an important source of dissolved amino acids and cell wall compounds J. Mar. Biol. Assoc. UK, 86, 605-612, 2006.

Miller, A. G., Espie, G. S., and Canvin, D. T.: Physiological aspects of CO_2 and HCO_3^- transport by cyanobacteria: a review, Can. J. Bot., 68, 1291-1302, https://doi.org/10.1139/b90-165, 1990.

Millo, C., Dupraz, S., Ader, M., Guyot, F., Thaler, C., Foy, E., and Ménez, B.: Carbon isotope fractionation during calcium carbonate precipitation induced by ureolytic bacteria, Geochim. Cosmochim. Acta., 98, 107-124, https://doi.org/10.1016/j.gca.2012.08.029, 2012.

Möller, H.: The influence of Mg^{2+} on the formation of calcareous deposits on a freely corroding low carbon steel in seawater, Corros. Sci., 49, 1992-2001, https://doi.org/10.1016/j.corsci.2006.10.011, 2007.

Morse, J. W., Gledhill, D. K., and Millero, F. J.: $CaCO_3$ precipitation kinetics in waters from the great Bahama bank: Implications for the relationship between bank hydrochemistry and whitings, Geochim. Cosmochim. Acta., 67, 2819-2826, http://doi.org/10.1016/S0016-7037(03)00103-0, 2003.

Morse, J. W., Arvidson, R. S., and Lüttge, A.: Calcium carbonate formation and dissolution, Chem. Rev., 107, 342-381, https://doi.org/10.1021/cr050358j, 2007.

Nguyen Dang, D., Gascoin, S., Zanibellato, A., G. Da Silva, C., Lemoine, M., Riffault, B., Sabot, R., Jeannin, M., Chateigner, D., and Gil, O.: Role of brucite dissolution in calcium carbonate precipitation from artificial and natural seawaters, Cryst. Growth. Des., 17, 1502-1513, https://doi.org/10.1021/acs.cgd.6b01305, 2017.

Nothdurft, L. D., Webb, G. E., Buster, N. A., Holmes, C. W., Sorauf, J. E., and Kloprogge, J. T.: Brucite microbialites in living coral skeletons: Indicators of extreme microenvironments in shallow-marine settings, Geology, 33, 169-172, https://doi.org/10.1130/g20932.1, 2005.

Obst, M., Dynes, J. J., Lawrence, J. R., Swerhone, G. D. W., Benzerara, K., Karunakaran, C., Kaznatcheev, K., Tyliszczak, T., and Hitchcock, A. P.: Precipitation of amorphous $CaCO_3$ (aragonite-like) by cyanobacteria: A STXM study of the influence of EPS on the nucleation process, Geochimi. Cosmochimi. Acta., 73, 4180-4198, http://doi.org/10.1016/j.gca.2009.04.013, 2009a.

Obst, M., Wehrli, B., and Dittrich, M.: $CaCO_3$ nucleation by cyanobacteria: laboratory evidence for a passive, surface-induced mechanism, Geobiology, 7, 324-347, https://doi.org/10.1111/j.1472-4669.2009.00200.x, 2009b.

Orange, F., Chabin, A., Gorlas, A., Lucas-Staat, S., Geslin, C., Le Romancer, M., Prangishvili, D., Forterre, P., and Westall, F.: Experimental fossilisation of viruses from extremophilic Archaea, Biogeosciences, 8, 1465-1475, https://doi.org/10.5194/bg-8-1465-2011, 2011.

Pacton, M., Wacey, D., Corinaldesi, C., Tangherlini, M., Kilburn, M. R., Gorin, G. E., Danovaro, R., and Vasconcelos, C.: Viruses as new agents of organomineralization in the geological record, Nat. Commun., 5, 4298-4298, https://doi.org/10.1038/ncomms5298, 2014..

Patel, A., Noble, R. T., Steele, J. A., Schwalbach, M. S., Hewson, I., and Fuhrman, J. A.: Virus and prokaryote enumeration from planktonic aquatic environments by epifluorescence microscopy with SYBR Green I, Nat. Protoc., 2, 269, https://doi.org/10.1038/nprot.2007.6, 2007.

Peng, X., Xu, H., Jones, B., Chen, S., and Zhou, H.: Silicified virus-like nanoparticles in an extreme thermal environment: implications for the preservation of viruses in the geological record, Geobiology, 11, 511-526, https://doi.org/10.1111/gbi.12052, 2013.

Perri, E., Tucker, M. E., Słowakiewicz, M., Whitaker, F., Bowen, L., and Perrotta, I. D.: Carbonate and silicate biomineralization in a hypersaline microbial mat (Mesaieed sabkha, Qatar): Roles of bacteria, extracellular polymeric substances and viruses, Sedimentology, 1213-1245, https://doi.org/10.1111/sed.12419, 2017.

Planavsky, N., Reid, R. P., Lyons, T. W., Myshrall, K. L., and Visscher, P. T.: Formation and diagenesis of modern marine calcified cyanobacteria, Geobiology, 7, 566-576, https://doi.org/10.1111/j.1472-4669.2009.00216.x, 2009.

Ridgwell, A., and Zeebe, R. E.: The role of the global carbonate cycle in the regulation and evolution of the Earth system, Earth. Planet. Sci. Lett., 234, 299-315, http://doi.org/10.1016/j.epsl.2005.03.006, 2005.

Riding, R.: Cyanobacterial calcification, carbon dioxide concentrating mechanisms, and Proterozoic–Cambrian changes in atmospheric composition, Geobiology, 4, 299-316, https://doi.org/10.1111/j.1472-4669.2006.00087.x, 2006.

Riding, R.: Calcified Cyanobacteria, in: Encyclopedia of Geobiology, edited by: Reitner, J., and Thiel, V., Springer Netherlands, Dordrecht, 211-223, 2011.

Riding, R.: A Hard Life for Cyanobacteria, Science, 336, 427-428, https://doi.org/10.1126/science.1221055, 2012.

Rodriguez-Blanco, J. D., Shaw, S., and Benning, L. G.: How to make 'stable' ACC: protocol and preliminary structural characterization, Mineral. Mag., 72, 283-286, https://doi.org/10.1180/minmag.2008.072.1.283, 2008.

Rohwer, F., and Thurber, R. V.: Viruses manipulate the marine environment, Nature, 459, 207-212, https://doi.org/10.1038/nature08060, 2009.

Semesi, I. S., Kangwe, J., and Björk, M.: Alterations in seawater pH and CO_2 affect calcification and photosynthesis in the tropical coralline alga, Hydrolithon sp. (Rhodophyta), Estuar. Coast. Shelf Sci., 84, 337-341, http://doi.org/10.1016/j.ecss.2009.03.038, 2009.

Suttle, C. A., and Chan, A. M.: Dynamics and distribution of cyanophages and their effect on marine *Synechococcus* spp, Appl. Environ. Microb., 60, 3167-3174, 1994.

Suttle, C. A.: Viruses in the sea, Nature, 437, 356-361, https://doi.org/10.1038/nature04160, 2005.

Suttle, C. A.: Marine viruses—major players in the global ecosystem, Nat. Rev. Microbiol., 5, 801-812, https://doi.org/10.1038/nrmicro1750, 2007.

Tesson, B., Gaillard, C., and Martin-Jézéquel, V.: Brucite formation mediated by the diatom Phaeodactylum tricornutum, Mar. Chem., 109, 60-76, https://doi.org/10.1016/j.marchem.2007.12.005, 2008.

Weiner, S., and Addadi, L.: Crystallization pathways in biomineralization, Annu. Rev. Mater. Res., 41, 21-40, https://doi.org/10.1146/annurev-matsci-062910-095803, 2011.

Weitz, J. S., and Wilhelm, S. W.: Ocean viruses and their effects on microbial communities and biogeochemical cycles, F1000 biology reports, 4, https://doi.org/10.3410/B4-17, 2012.

Wright, D. T., and Oren, A.: Nonphotosynthetic bacteria and the formation of carbonates and evaporites through time, Geomicrobiol. J., 22, 27-53, https://doi.org/10.1080/01490450590922532, 2005.

Yang, Z.-N., Li, X.-M., Umar, A., Fan, W.-H., and Wang, Y.: Insight into calcification of *Synechocystis* sp. enhanced by extracellular carbonic anhydrase, RSC Adv., 6, 29811-29817, https://doi.org/10.1039/C5RA26159G, 2016.

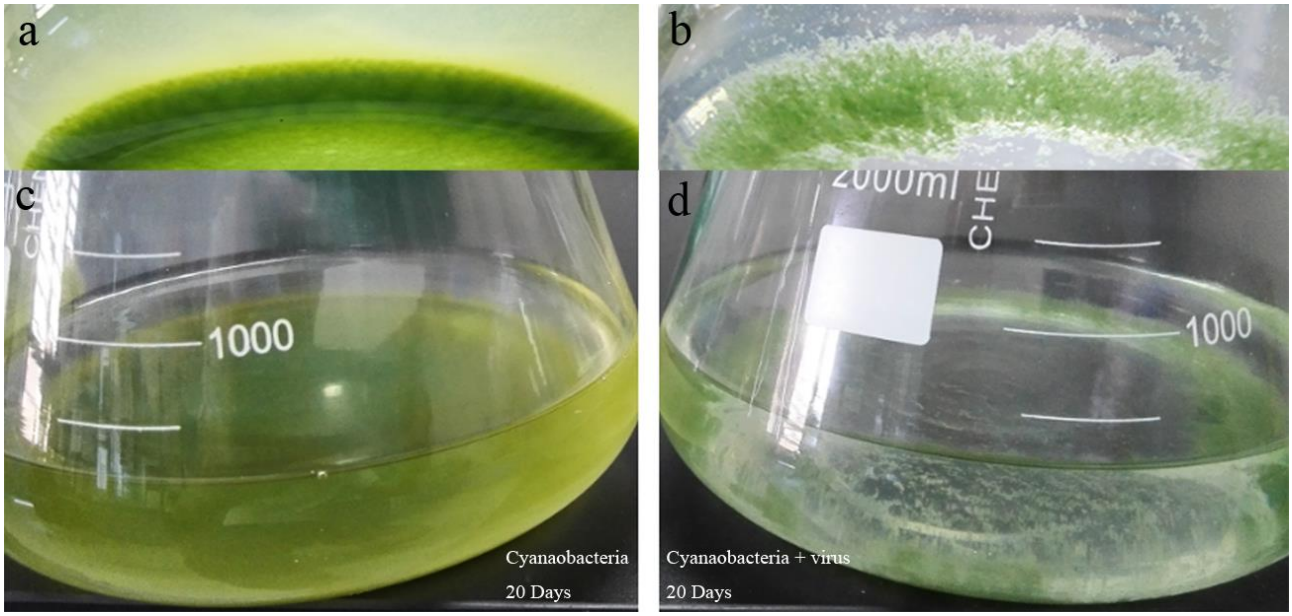

Figure 1: Photos of the culture medium at the end of the experiments. (a and c) without inoculation of the virus. (b and d) white precipitates are evident in viral lysis of cyanobacteria.

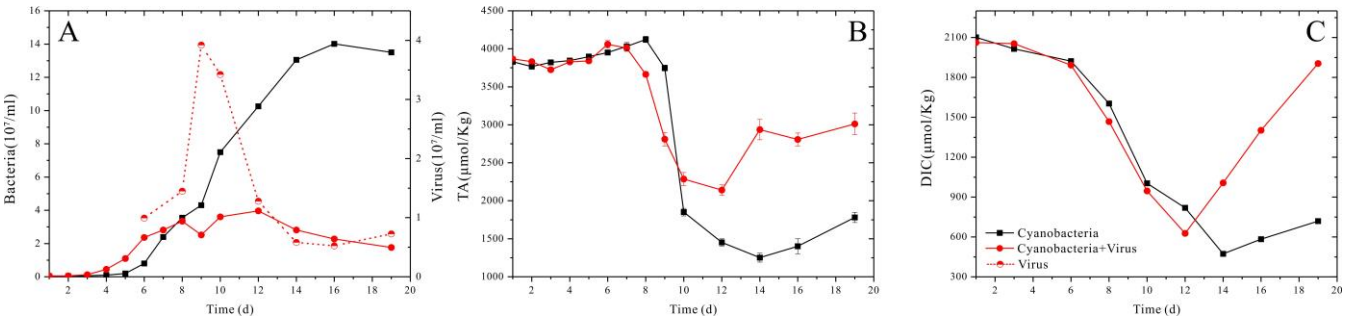

Figure 2: Changes in the solution bacteria and virus concentration (a), total alkalinity (b) and dissolved inorganic carbon (c)

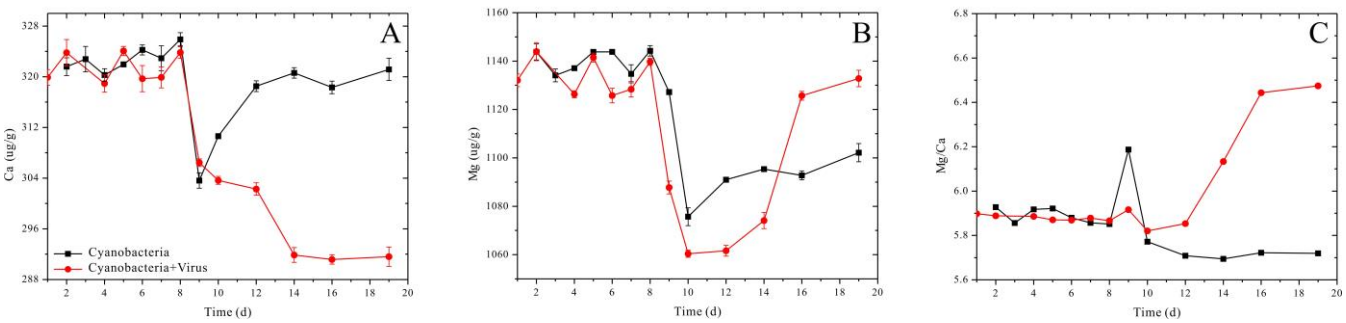

Figure 3: Changes in the solution calcium concentration (a), magnesium concentration (b) and Ma/Ca atomic ratio (c).

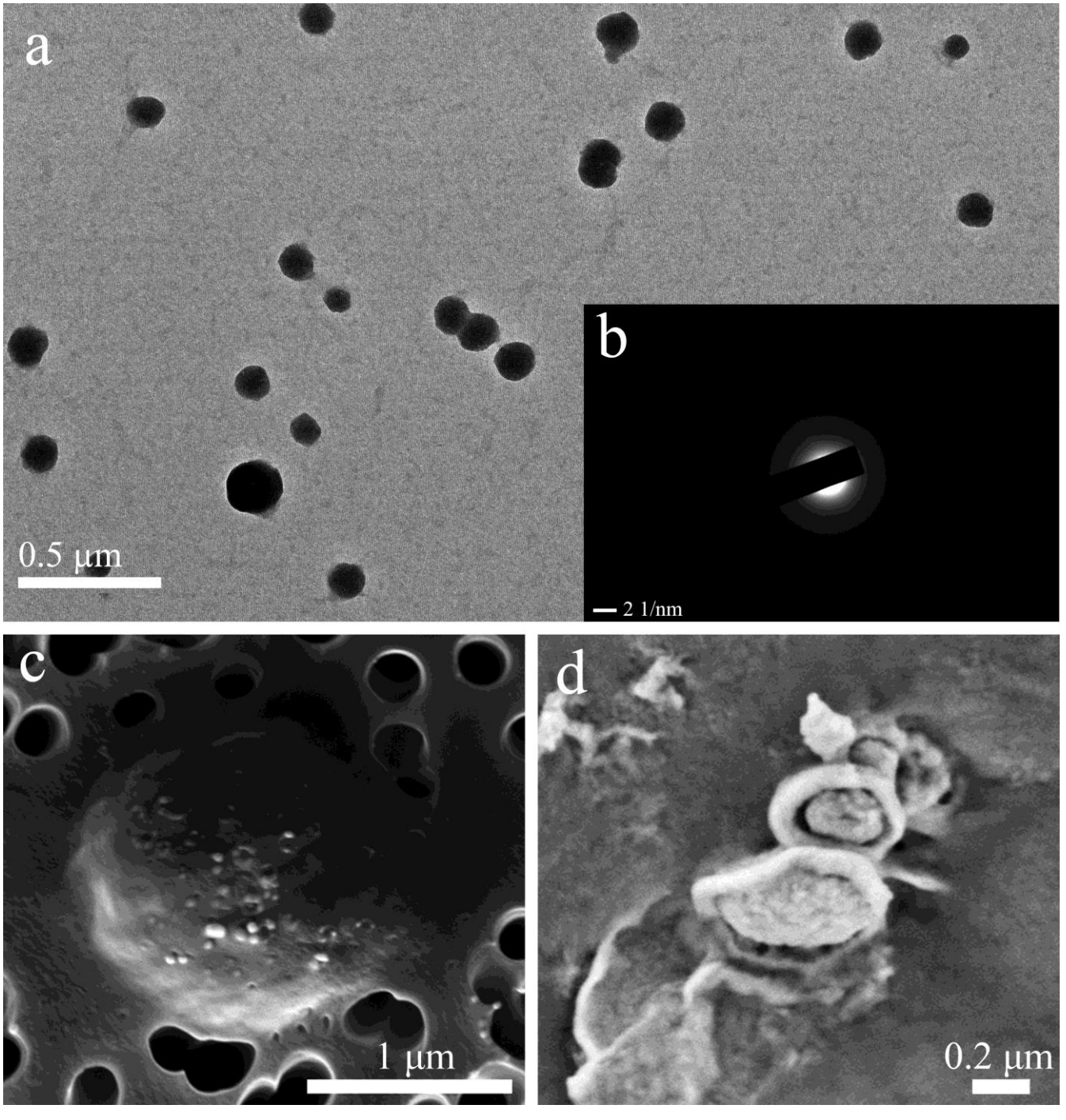

Figure 4: Electron microscope images show the formation of ACC nanoparticles in the viral lysate. (a) Nanoparticles with a diameter of approximately 50-200 nm are scattered in the viral lysate. The insert at the bottom right image (b) shows a selected area of the electron diffraction pattern of ACC, revealing only diffuse rings, related to poorly ordered materials (c) Back scattered-

electron imaging photomicrographs of host cells infected by virus and mineral particles. (d) Nano-particles with an encrusted structure.

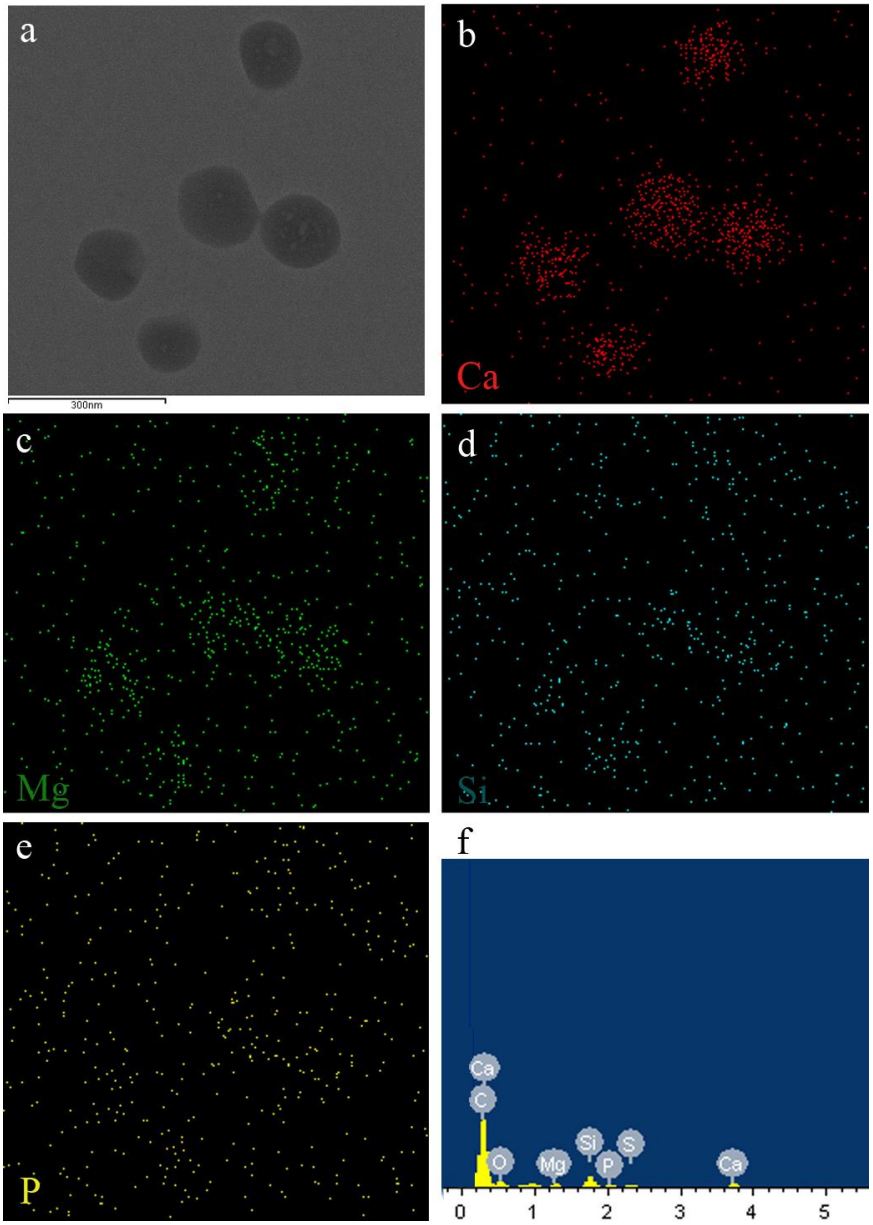

Figure 5: Chemical composition of ACC nanoparticles. (a) STEM images showing ACC nanoparticles. (b, c, d, e) XEDS maps of Ca, Mg, Si and P, respectively showing that ACC is composed mainly of Ca. EDS spectra of the nanoparticle shows a small peak of element P (f). However, the P signal from the STEM mapping is not consistent with the nanoparticles (e).

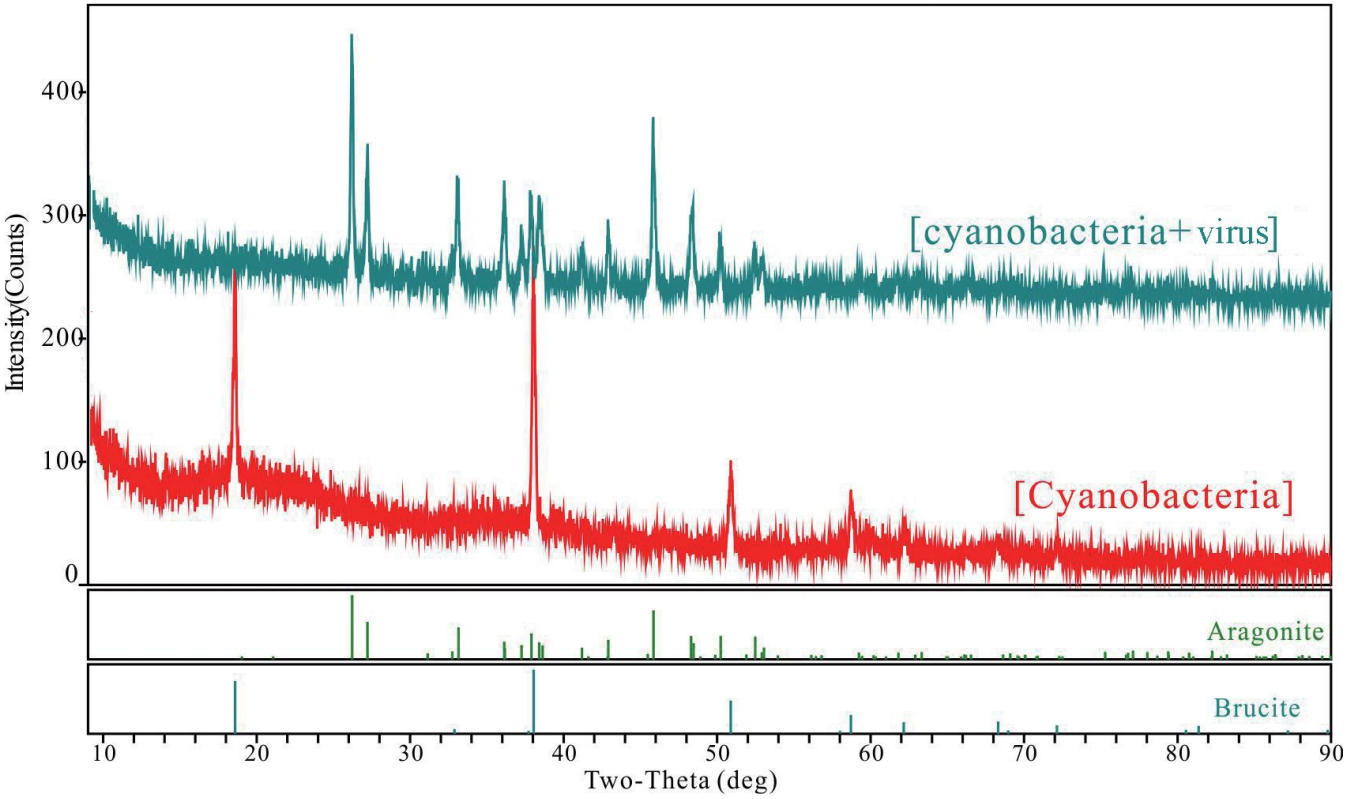

Figure 6: Typical X-ray diffraction patterns collected for each polymorph that formed in this study.

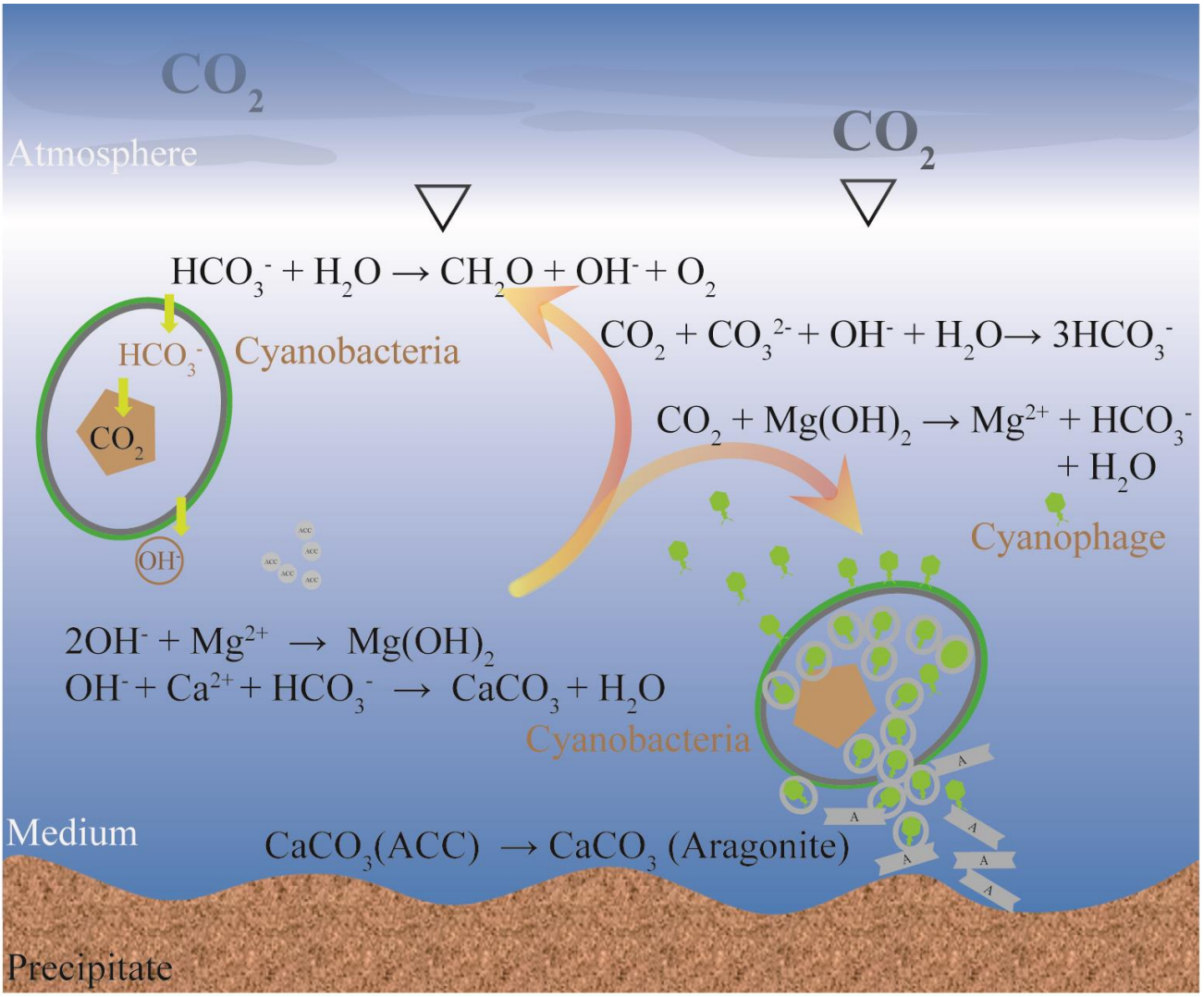

Figure 7: Formation model of the carbonate mineral induced by viral lysis of the cyanobacteria. Although the chemical environment may be favorable for mineral precipitation during photosynthesis, it is unable to facilitate mineralization to the extent that stable $CaCO_3$ precipitates are formed. During the viral lysis of cyanobacteria, there are a few percentages of uninfected cells that require bicarbonate, $Mg(OH)_2$ dissolved to neutralize the dissolution of CO_2. Viral lysis of cyanobacteria thus construct a calcification environment where carbonate is the dominant inorganic carbon species. Numerous virus particles available in lysate may coprecipitate with the calcium carbonate.

Table 1 Composition of the artificial seawater (modified F/2 media, final pH was adjust to 8). Regents are purchased from Sinopharm and Sigma-Aldrich

Chemical	Amount (g/L)	Chemical	Amount (10^{-5} g/L)
NaCl	21.19	**$CuSO_4 \cdot 5H_2O$**	0.98
Na_2SO_4	3.55	**$ZnSO_4 \cdot 7H_2O$**	2.20
KCl	0.60	**$CoCl \cdot 6H_2O$**	1.00
$NaHCO_3$	0.29	**$MnCl_2 \cdot 4H_2O$**	18.0
KBr	0.09	**$Na_2MoO_4 2H_2O$**	0.63
H_3BO_3	0.02	**$Na_2EDTA \cdot 2H_2O$**	436
NaF	0.003	**$FeCl_3 \cdot 6H_2O$**	315
$MgCl_2$ $6H_2O$	9.59	**vitamin B1**	0.01
$CaCl_2$	1.01	**Vitamin Biotin**	0.00005
$SrCl_2$ $6H_2O$	0.02	**Vitamin B12**	0.00005
$NaNO_3$	0.075		
NaH_2PO_4 H_2O	0.005		
Na_2SiO_3 $9H_2O$	0.03		

Table 2 Saturation indices calculated from culture system by PHREEQC.

	Time (d) / saturation index	6	8	10	12	14	16
Cyanbacteria	pH	9.56	9.96	8.66	8.95	9.32	9.29
	Aragonite	1.34	1.35	0.56	0.69	0.65	0.73
	Brucite	0.34	1.15	-1.47	-0.89	-0.15	-0.2
	ACC	-0.72	-0.71	-1.50	-1.37	-1.41	-1.33
	vaterite	0.92	0.93	0.14	0.27	0.23	0.31
Cyanbacteria + Virus	pH	9.65	9.85	8.87	9.89	9.93	9.74
	Aragonite	1.36	1.3	0.68	0.92	1.12	1.1
	Brucite	0.52	0.92	-1.06	0.93	1.06	-0.02
	ACC	-0.70	-0.76	-1.38	-1.14	-0.94	-0.96
	vaterite	0.94	0.88	0.26	0.50	0.70	0.68